system has to travel through the broad region of the phase coexistence and might be lost by the time it arrives at the surface of the system. This is particularly important for strongly interacting probes like antimatter [Hei84, Sub85] and strangeness [Raf82, Koc83], which will be subject to the complicated hadronic reaction dynamics which has to be tackled on top of the hard problems connected to the confinement problem itself. We will in the next chapter develop the theoretical framework necessary for the quantitative description of the collision dynamics.

II. Many Body Theory of Nuclear Collisions — Finite Time Scales in Finite Systems

II.1. Microscopic kinetic theory

II.1.1. Hierarchy of theories

A comprehensive theory of nuclear collisions at high energies should describe relativistic quantum mechanical wave packets interacting simultaneously with all other wave packets via the correct two nucleon interaction for scattering inside the medium. Although this already neglects correlations, such a quantum mechanical treatment has not yet been attempted, but even the formulation of the interaction itself poses formidable problems. A natural suggestion —and one that has been very successfully employed in the cascade calculations — is to use measured free N–N cross sections as the primary physical input. This is legitimate if only binary N–N interactions occur and the scattered nucleons always reach their asymptotic states before encountering another nucleon; in other words: if the system is dilute. The cascade models and all other models that assume N–N scattering to occur at a point require diluteness.

If one does not want to assume diluteness, the simultaneous interaction of many nucleons has to be allowed. In this case scattering can no longer be described in terms of asymptotic states and cross sections, but an explicit interaction potential is required. The models that use this approach generally describe the nucleon motion in terms of classical trajectories and forces and are therefore often called classical dynamics models. In the relativistic realm there are huge problems even with the formulation of the theory — although it is possible to replace the Dirac equations by relativistic Newton's equations, the meson fields do not obey classical equations even approximately. The only possibility to obtain a solvable model seems to be to ignore second quantization and treat the meson fields classically. The model which comes closest to solving the many-body aspect exactly are the non-relativistic equations of motion with two body potentials, which are actually solvable. The major problem associated with this approach is that classical potentials provide only a poor approximation to N–N scattering and to nuclear binding properties. We will start the discussion of dynamical models with this approach.

II.1.2. Newtonian force model — The classical limit

Consider the classical Γ space description of an A body system with fixed degrees of freedom: we have in mind the colliding system of $A = A_P + A_T$ nucleons. Recall that Γ space is a $6A$ dimensional phase space and the state of the system is represented by one point in this space. Let $\rho(\boldsymbol{r}_1, \ldots, \boldsymbol{r}_A, \boldsymbol{p}_1, \ldots, \boldsymbol{p}_A, t)\, \mathrm{d}\Gamma$ be the probability to find the system at the point $(\boldsymbol{r}_1, \ldots, \boldsymbol{r}_A, \boldsymbol{p}_1, \ldots, \boldsymbol{p}_A)$ in Γ space at time t: ρ is the A-body distribution function. The classical Liouville equation then follows from considering ρ as a probability fluid:

$$\frac{\partial \rho}{\partial t} + \sum_{i=1}^{A} \left(\frac{\partial}{\partial \boldsymbol{r}_i} \cdot (\rho \dot{\boldsymbol{r}}_i) + \frac{\partial}{\partial \boldsymbol{p}_i} \cdot (\rho \dot{\boldsymbol{p}}) \right) = 0$$

$$= \frac{\partial \rho}{\partial t} + \sum_{i=1}^{A} \left(\dot{\boldsymbol{r}}_i \cdot \frac{\partial \rho}{\partial \boldsymbol{r}_i} + \dot{\boldsymbol{p}}_i \cdot \frac{\partial \rho}{\partial \boldsymbol{p}_i} \right). \tag{II.1}$$

Hamilton's equations then imply that:

$$\partial \rho / \partial t = \{H, \rho\}. \tag{II.2}$$

This is the classical Liouville equation which describes a microcanonical ensemble. For equilibrium, we have the condition $\{H, \rho\} = 0$.

The Newtonian Force Model (also dubbed "Molecular Dynamics" or "Equation of Motion" approach) in nuclear physics consists in solving Newton's or Hamilton's equations of motion for the A interacting nucleons. This is a theory for the full non-equilibrium classical situation. The NFM is thus more fundamental than a kinetic equation approach since it solves the Liouville equation.

Of course, there are then no quantum effects in this model. However, one does have information of the A body classical distribution function. One must however use a classical potential to study heavy ion systems. Over the years, nuclear physics has been driven to more and more complicated nucleon–nucleon interactions culminating e.g. in the Bonn and Paris potentials in order to accommodate the spin, isospin, etc. degrees of freedom.

A simple ansatz for a classical central potential that acts between each nucleon and all other $A - 1$ nucleons consists of repulsive and attractive Yukawa terms [Bod77, Wil77, Mol84a]:

$$V = (V_{\mathrm{R}} \exp(-k_{\mathrm{R}} \cdot r) - V_{\mathrm{A}} \exp(-k_{\mathrm{A}} \cdot r))/r. \tag{II.3}$$

The parameters in the potential are chosen in a compromise between reproducing in a completely classical calculation the n–p differential scattering cross section at large angles $\theta_{\mathrm{C.M.}} \approx 90°$ (which influences the transverse momentum transfer the most) and at the same time giving reasonable binding energies and stable nuclei. Recall that the cross section is calculated classically from:

$$\frac{\mathrm{d}\sigma}{\mathrm{d}\Omega} = \frac{b}{\sin(\theta)} \frac{\mathrm{d}b}{\mathrm{d}\theta}. \tag{II.4}$$

The experimental differential cross section is thus hard to obtain because of the purely quantum mechanical diffraction and exchange effects. A meaningful quantity to fit is the viscosity moment of the scattering cross section:

$$\sigma_{\mathrm{v}} = 2\pi \int \sigma(\theta) \sin^2(\theta) \, \mathrm{d}(\cos(\theta)) \tag{II.5}$$

which is related to the viscosity and thermal conductivity in a Boltzmann equation approach [Bod77].

In the NFM approach [Mol84a], nuclei are described as an ensemble of protons and neutrons initially distributed randomly throughout a sphere with the nuclear radius $R = 1.2\,\mathrm{A}^{1/3}$. Some cutoff on

the interparticle positions, say 1.2 fm, must be imposed so that nucleons do not evaporate with large amounts of energy due to the classical potential. The nucleons are also given random Fermi momenta. To numerically simulate a collision process, the nuclei are Galilei boosted with the respective center of mass momenta at given impact parameter. The Newtonian equations of motion are integrated using a fourth order Adams–Moulton predictor-corrector method. Energy conservation to better than 1% is demanded. Then Newton's equations of motion are solved for the $A = A_P + A_T$ interacting nucleons:

$$\boldsymbol{F}_i = \mathrm{d}\boldsymbol{p}_i/\mathrm{d}t = -\partial U/\partial \boldsymbol{r}_i \tag{II.6}$$

where $U(r_i) = \Sigma_{i<j}^{A} V(r_{ij})$.

We show in fig. II.1 how a Nb + Nb collision at 400 MeV/nucleon evolves in this approach. Note the strong bounce-off or side-splash of nuclear matter [Mol84a]. Calculations for many other systems have been done by other authors [Bod77, Wil77, Bod80, Bod81, Wil78, Cal79].

The main problem with this NFM approach is, of course, that classical potentials can provide only a poor approximation to n–n scattering and nuclear binding properties. For example, one finds that in

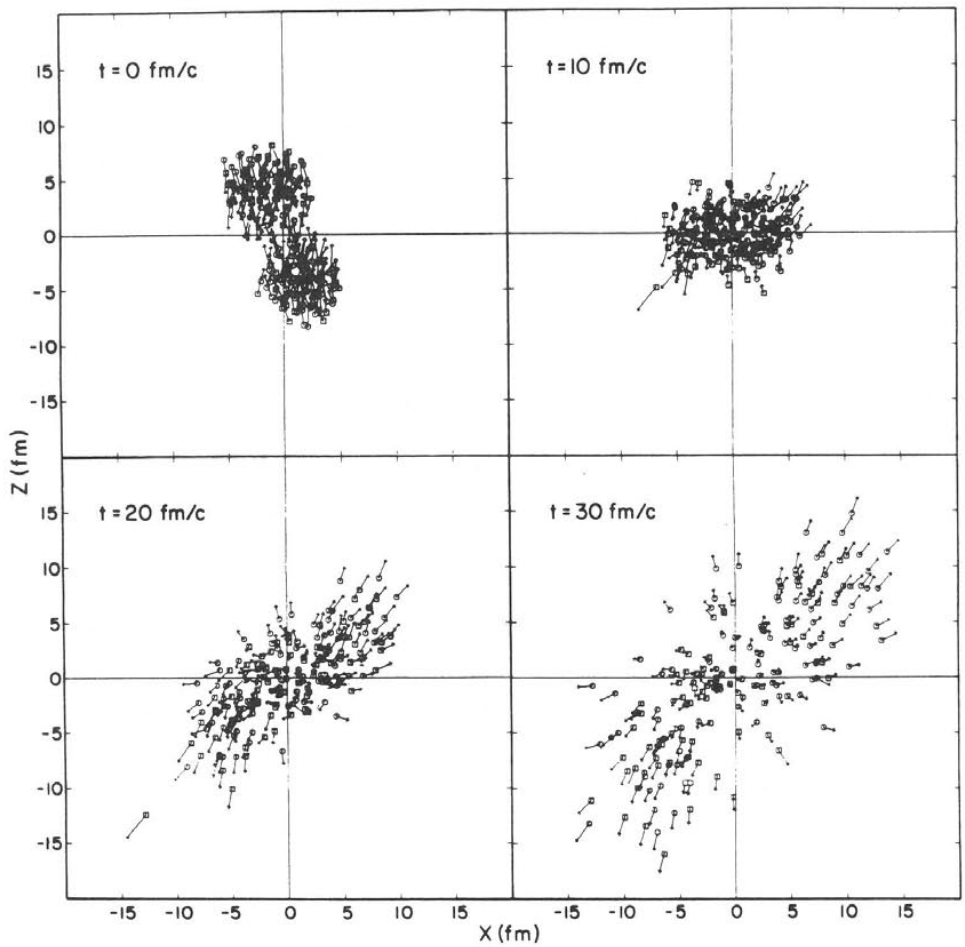

Fig. II.1. Nb(400 MeV/nucleon) + Nb as a function of time in the Newtonian Force Model: strong collective flow is caused by the short range repulsive nuclear force [Mol85a].

order to simulate nuclear saturation, the two body potential must have a long range repulsive tail, as had been suggested earlier [Wil78]. However, the NFM do come closest to solving the many-body aspect and probing finite range effects of the repulsive core. And it is interesting that such a classical approach can with partial success describe heavy ion interactions in the intermediate energy range. In the relativistic generalization, there are additional complications [Kun81]: One can write down relativistic Newtonian equations in place of the Dirac equations; but the meson fields do not obey classical equations. One possibility is to ignore second quantization and consider the meson fields as classical radiation fields, thereby studying also retardation effects. We would like to point out that recently a "Quantum Molecular Dynamics" approach has been developed [Aic86], which incorporates the most prominent quantum physics into the N-body molecular dynamics method.

II.1.3. N-body density matrix and TDHF

To solve even the non-relativistic quantum A body nuclear physics problem, one has to solve the time dependent Schrödinger equation [Sch25]:

$$i\hbar \partial \Psi / \partial t = H\Psi \tag{II.7}$$

$$\Psi = \Psi(1, 2, \ldots, A, t) \tag{II.8}$$

is the time dependent many-body wave function, A is the total number of nucleons, and H is the many body Hamiltonian. This is in general an impossible task just as the complete relativistic problem is.

Recall that an approach to the static many body problem for atomic electrons is Hartree's theory of the selfconsistent field [Har27]. There one uses a product of single particle wave functions, solves the single particle wave equation neglecting the interaction, and secondly includes interactions and solves for new single particle wave functions. These two steps are iterated until one achieves consistency between the field and the electron density.

Static Hartree Fock theory differs in the inclusion of an exchange term [Foc30]. The many-body wave function is there approximated as a Slater determinant of single particle wave functions. The Hartree Fock Hamiltonian contains the Hartree field and a non-local exchange term. Again one proceeds iteratively to achieve consistency between the field and the density. The HF state is a Fermi sea of particles with a sharp Fermi surface, since in constructing the HF determinant one selects the A lowest energy wave functions. Thus one may regard the HF state as the particle hole vacuum $|\ \rangle$. Hole states are occupied single particle states and particle states are unoccupied [Row70].

Static Hartree Fock theory has had much success in the shell models of electrons and later nucleons. In heavy ion physics, however, one has a time dependent problem of A colliding nucleons. The complete nuclear wave function Ψ contains lots of information — perhaps more than we will ever need or be able to use. One therefore is justified in making some approximations to get a tractable time dependent Hartree Fock theory.

Nucleons are bound together solely by their mutual interaction: there is no external central field as with atomic electrons. The HF method is an approximation for reducing the problem of many interacting particles to one of non-interacting particles in a field. This neglects the residual interaction part of the nucleon–nucleon force. TDHF is used to describe excited states and to take account of the long range or field part of the residual interaction.

Recall that TDHF can be derived in the formalism of second quantization [Koo75]. Let

$$|abc\ldots\rangle = \frac{1}{\sqrt{A!}} \sum_{(ab\ldots.)} \psi_a \psi_b \ldots \operatorname{sgn}(abc\ldots) \tag{II.9}$$

be the Slater determinant. The subscripts label space, spin, isospin, etc. Define the particle creation and destruction operators $a_i^\dagger$ and a_i, respectively. Antisymmetry and the Pauli principle yield the anti-commutation relations:

$$\{a_i^\dagger, a_j^\dagger\} = 0 \qquad \text{and} \qquad \{a_i^\dagger, a_j\} = \delta_{ij} . \tag{II.10}$$

The state Ψ of the nucleus is then a linear combination of such Slater determinant kets.

The many body Hamiltonian is

$$\begin{aligned} H &= T + V \\ &= \sum_{ij} T_{ij} a_i^\dagger a_j + \frac{1}{2} \sum_{ijkl} U_{ijkl} a_i^\dagger a_j^\dagger a_l a_k \end{aligned} \tag{II.11}$$

where the kinetic energy is a single particle operator and U is the two body interaction. The one body density matrix is

$$\rho_{ji} = \langle \Psi | a_i^\dagger a_j | \Psi \rangle . \tag{II.12}$$

The von Neumann equation

$$\mathrm{i}\hbar \, \mathrm{d}\rho / \mathrm{d}t = \langle \Psi | [a_i^\dagger a_j, H] | \Psi \rangle \tag{II.13}$$

follows from the Schrödinger equation and the assumption that H is Hermitean. After inserting the many body Hamiltonian and considerable algebra, this time dependent density equation will not reduce to a pure one body equation. The two body force couples ρ to $\rho^{(2)}$, the two body density matrix. This is the BBGKY hierarchy [Koo75]. The TDHF approximation is to assume that

$$\rho^{(2)}_{ijkl} = \rho_{jk}\rho_{il} - \rho_{jl}\rho_{ik} . \tag{II.14}$$

This terminates the BBGKY hierarchy and yields the TDHF equation

$$\mathrm{i}\hbar \, \mathrm{d}\rho / \mathrm{d}t = [h, \rho] \tag{II.15}$$

where h is the HF Hamiltonian:

$$h = \sum_{ij} \left(T_{ij} + \sum_{kl} (V_{ikjl} - V_{iklj}) \rho_{lk} \right) . \tag{II.16}$$

It is not difficult to show that particle number, energy and Slater-determinantness are conserved in

TDHF [Koo75]. Furthermore, each of the single particle orbitals satisfies the time dependent Schrödinger equation with the HF Hamiltonian h.

TDHF has been applied with some success at energies up to 10 MeV/nucleon. Fusion, compound nucleus formation, dissipation, strongly damped collisions, shock wave propagation, and fragmentation are all found in TDHF [Bon76]. Beyond this range, mean field theory is not sufficient because of the lack of two body collisions and because the TDHF model assumes a long mean free path for the nucleons. The potential scattering of TDHF implies only a single particle viscosity so that the nuclei are rather transparent for $E_{C.M.} > E_F = 38$ MeV. This transparency is illustrated in fig. II.2 for Kr (85 MeV/nucleon) + Kr [Stö80a].

To go beyond TDHF, consider that some perturbing two body interaction causes particles to scatter from their unperturbed orbitals. In first order perturbation theory, the perturbed wave function is:

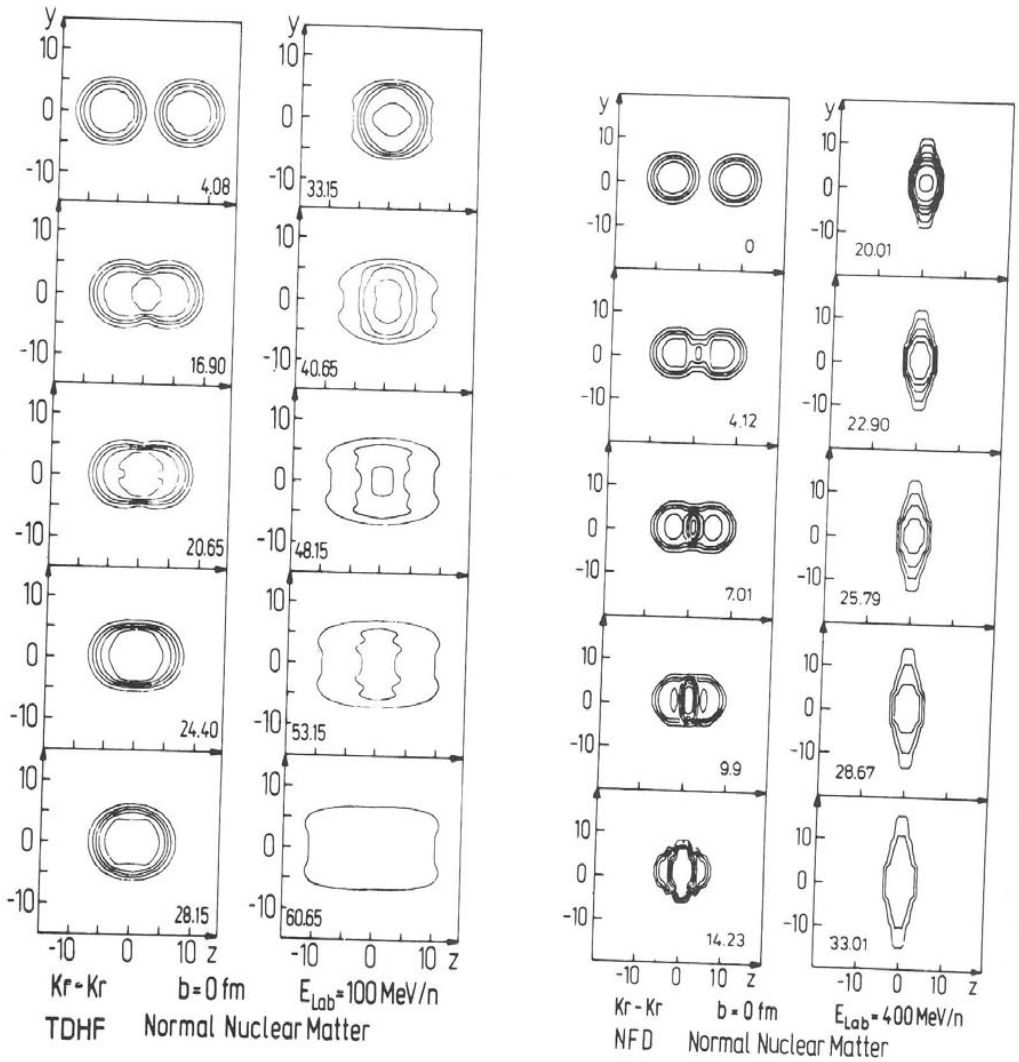

Fig. II.2. Contour plots of the baryon density in the scattering plane for a TDHF calculation of Kr + Kr at $b = 0$ fm and 100 MeV/nucleon incident energy (left) and the corresponding system at $E_{Lab} = 400$ MeV/nucleon as calculated in the fluid dynamical model [Stö80a].

$$|\Psi\rangle = |\Psi_0\rangle + \frac{1}{\mathrm{i}\hbar} \sum_{klk'l'} \int \mathrm{d}t\, \mathrm{e}^{\mathrm{i}\omega t} V_{k'l'kl} a^\dagger_{k'} a^\dagger_{l'} a_l a_k |\Psi_0\rangle$$

$$= |\Psi_0\rangle - \sum_{klk'l'} \frac{\mathrm{e}^{\mathrm{i}\omega t} - 1}{\hbar\omega} V_{k'l'kl} a^\dagger_{k'} a^\dagger_{l'} a_l a_k |\Psi\rangle \,. \tag{II.17}$$

The density matrix then evolves according to the von Neumann equation:

$$\mathrm{d}\rho_{ii}/\mathrm{d}t = \frac{1}{\mathrm{i}\hbar} \langle\Psi| a^\dagger_i [a_i, V] + [a^\dagger_i, V] a_i |\Psi\rangle \,. \tag{II.18}$$

Proceeding from here is complicated by the fact that one has to evaluate octupole Fock space operators. Let us thus consider the one body perturbing interaction as an illustrative example [Ber84b]. Then the first order perturbed wave function is:

$$|\Psi\rangle = |\Psi_0\rangle - \sum_{kk'} \frac{\mathrm{e}^{\mathrm{i}\omega t} - 1}{\hbar\omega} V_{k'k} a^\dagger_{k'} a_k |\Psi_0\rangle \,. \tag{II.19}$$

In the one body case, it is easily shown using the anti-commutation rules that

$$[a_i, V] = \sum_j V_{ji} a_j \qquad \text{and} \qquad [a^\dagger_i, V] = -\sum_j V_{ij} a^\dagger_j \,. \tag{II.20}$$

With the additional assumption that the one body density matrix is diagonal

$$\rho_{ji} = n_i \delta_{ij} \tag{II.21}$$

we have for the occupation number n_i the equation

$$\mathrm{d}n_i/\mathrm{d}t = \frac{1}{\mathrm{i}\hbar} \sum_j V_{ij} \langle\Psi| a^\dagger_i a_j - a^\dagger_j a_i |\Psi\rangle \,. \tag{II.22}$$

Substituting the bra and ket first order perturbed wave functions, one gets terms of first, second, and third order in V. The first order terms are already in the mean field and the third order terms may be neglected with respect to the second order ones. A typical second order term is

$$\langle\Psi_0| a^\dagger_i a_j a^\dagger_{l'} a_l |\Psi_0\rangle = \langle\Psi_0| a^\dagger_i (\delta_{jl'} - a^\dagger_{l'} a_j) a_l |\Psi_0]$$

$$= \rho_{li}\delta_{jl'} - \rho_{ljl'i}$$

$$= \rho_{li}\delta_{jl'} - \rho_{jl'}\rho_{li} + \rho_{ji}\rho_{ll'}$$

$$= n_i(1 - n_j)\delta_{li}\delta_{jl'} + n_i n_l \delta_{ij}\delta_{ll'} \,. \tag{II.23}$$

Putting all this together and collecting terms, one finds that

$$\mathrm{d}n_i/\mathrm{d}t = \frac{1}{\hbar^2}\sum_j [2V_{ij}\sin(\omega_{ji}t)/\omega_{ji}]\,[n_j(1-n_i)-n_i(1-n_j)]$$

$$= \frac{2\pi}{\hbar}\sum_j V_{ij}^2\,\delta(E_j-E_i)\,[n_j(1-n_i)-n_i(1-n_j)] \qquad \text{(II.24)}$$

where in the last step we extend the time limit to infinity and make use of one definition of the delta function. In the two body case, one expects by analogy the corresponding equation:

$$\mathrm{d}n_i/\mathrm{d}t = \frac{2\pi}{\hbar}\sum_{ji'j'} V_{ijj'i'}^2\,\delta(E_{i'}+E_{j'}-E_i-E_j)[n_{i'}n_{j'}(1-n_i)(1-n_j)-n_in_j(1-n_{i'})(1-n_{j'})]\,. \qquad \text{(II.25)}$$

This then provides some plausible justification for Uehling and Uhlenbeck's original ansatz for a collision term [Ueh33].

II.1.4. The Vlasov–Uehling–Uhlenbeck equation

One way to include two body collisions is thus to couple to the TDHF equation a master equation involving the occupation probabilities of the single particle states n_i. The delta function which we find in the previous derivation is only present at the limit of vanishing single particle widths [Rem84]. We now replace the summation on the discrete single particle levels by continuous integrals over momenta:

$$\sum_{ji'j'} \to \int \mathrm{d}^3p_2\,\mathrm{d}^3p_1'\,\mathrm{d}^3p_2'/(2\pi\hbar)^3\,. \qquad \text{(II.26)}$$

Furthermore, the continuous analog of the occupation probability is the Wigner function

$$f(\boldsymbol{p},\boldsymbol{r}) = \int \mathrm{d}^3s\,\exp(\mathrm{i}\boldsymbol{p}\cdot\boldsymbol{s}/\hbar)\,\rho_{r+s/2,\,r-s/2} = \int \mathrm{d}^3q\,\exp(-\mathrm{i}\boldsymbol{q}\cdot\boldsymbol{r}/\hbar)\,\rho_{p+q/2,\,p-q/2} \qquad \text{(II.27)}$$

which has the properties that

$$\rho(\boldsymbol{r}) = \int \mathrm{d}^3p\,f(\boldsymbol{p},\boldsymbol{r})/(2\pi\hbar)^3 \qquad \text{and} \qquad \rho(\boldsymbol{p}) = \int \mathrm{d}^3r\,f(\boldsymbol{p},\boldsymbol{r})/(2\pi)^3\,. \qquad \text{(II.28)}$$

One can also eliminate the matrix element $\langle \boldsymbol{p}_1\boldsymbol{p}_2|V|\boldsymbol{p}_1'\boldsymbol{p}_2'\rangle$ with the Born approximation:

$$\langle p_1p_2|V|p_1'p_2'\rangle^2 = (2\pi\hbar^2/\mu)^2\,\mathrm{d}\sigma/\mathrm{d}\Omega\,. \qquad \text{(II.29)}$$

Then one obtains the Uehling–Uhlenbeck collision term

$$\left(\frac{\mathrm{d}f}{\mathrm{d}t}\right)_{\mathrm{coll}} = -\int \frac{\mathrm{d}^3p_2\,\mathrm{d}^3p_1'\,\mathrm{d}^3p_2'}{(2\pi)^6}\,\sigma v_{12}\,[ff_2(1-f_1')(1-f_2')-f_1'f_2'(1-f)(1-f_2)]\,\delta^3(p+p_2-p_1'-p_2') \qquad \text{(II.30)}$$

where we have replaced f_1 by f. Finally, we may also write the total derivative as:

$$\frac{\mathrm{d}f}{\mathrm{d}t}=\frac{\partial f}{\partial t}+\boldsymbol{v}\cdot\frac{\partial f}{\partial \boldsymbol{r}}+\frac{\mathrm{d}\boldsymbol{p}}{\mathrm{d}t}\cdot\frac{\partial f}{\partial \boldsymbol{p}}\cdot. \tag{II.31}$$

This last equation set equal to zero is the Vlasov equation. Finally combining these, we get the Vlasov–Uehling–Uhlenbeck equation:

$$\frac{\partial}{\partial t}f+\boldsymbol{v}\cdot\frac{\partial}{\partial \boldsymbol{r}}f-\nabla U\cdot\frac{\partial}{\partial \boldsymbol{p}}f=-\int\frac{\mathrm{d}^3p_2\,\mathrm{d}^3p_1'\,\mathrm{d}^3p_2'}{(2\pi)^6}\sigma v_{12}$$
$$\times[ff_2(1-f_1')(1-f_2')-f_1'f_2'(1-f)(1-f_2)]\delta^3(p+p_2-p_1'-p_2'). \tag{II.32}$$

The only input is now a potential U and the free nucleon–nucleon differential cross section σ. The Fermi–Dirac distribution, which is a solution of the Vlasov equation, is also the equilibrium solution of the collision term.

For the interaction U, a local Skyrme interaction is commonly used. Let us briefly review the Skyrme model. Skyrme's interaction can be written as a potential:

$$V=\sum_{ij}V_{ij}^{(2)}+\sum_{ijk}V_{ijk}^{(3)} \tag{II.33}$$

with two and three body parts. In configuration space, the two body part is:

$$V^{(2)}(\boldsymbol{r}-\boldsymbol{r}')=t_0(1+x_0P_\sigma)\,\delta(\boldsymbol{r}-\boldsymbol{r}')+\tfrac{1}{2}t_1(\boldsymbol{k}'^2\,\delta(\boldsymbol{r}-\boldsymbol{r}')+\delta(\boldsymbol{r}-\boldsymbol{r}')\boldsymbol{k}^2)$$
$$+t_2\boldsymbol{k}'\cdot\delta(\boldsymbol{r}-\boldsymbol{r}')\boldsymbol{k}+\mathrm{i}W_0\boldsymbol{k}'\cdot\delta(\boldsymbol{r}-\boldsymbol{r}')\boldsymbol{\sigma}\cdot\boldsymbol{k} \tag{II.34}$$

where

$$\boldsymbol{k}=(\partial/\partial\boldsymbol{r}-\partial/\partial\boldsymbol{r}')/2\mathrm{i}\qquad\text{and}\qquad\boldsymbol{k}'=\boldsymbol{k}^\dagger \tag{II.35}$$

are the relative momentum operators and

$$P_\sigma=\tfrac{1}{2}(1+\boldsymbol{\sigma}_1\cdot\boldsymbol{\sigma}_2) \tag{II.36}$$

is the spin exchange operator. Also, the three body part is

$$V^{(3)}(\boldsymbol{r}_1,\boldsymbol{r}_2,\boldsymbol{r}_3)=t_3\,\delta(\boldsymbol{r}_1-\boldsymbol{r}_2)\,\delta(\boldsymbol{r}_2-\boldsymbol{r}_3). \tag{II.37}$$

The Hartree–Fock method is usually used with this Skyrme interaction, so that the nuclear ground state is represented by a Slater determinant of single particle states Ψ. The expectation value of the total energy is then:

$$E=\langle\Psi|T+V|\Psi\rangle=\int H(\boldsymbol{r})\,\mathrm{d}^3r \tag{II.38}$$

where H is the Hartree–Fock functional energy density. For the Skyrme interaction, this energy density is an algebraic function of only three quantities: the nucleon density, kinetic energy density, and spin density:

$$\rho(\boldsymbol{r}) = \sum_{i=1}^{A} |\psi_i(\boldsymbol{r})|^2, \qquad \tau(\boldsymbol{r}) = \sum |\nabla\psi_i(\boldsymbol{r})|^2, \qquad \boldsymbol{J}(\boldsymbol{r}) = -\mathrm{i} \sum \psi_i^*(\boldsymbol{r}) \cdot (\nabla\psi_i(\boldsymbol{r}) \wedge \boldsymbol{\sigma}) . \tag{II.39}$$

For the case of a symmetric nucleus, $N = Z$, and if there is no Coulomb field then the densities for neutrons and protons are equal:

$$\rho_\mathrm{h} = \rho_\mathrm{p} = \tfrac{1}{2}\tau , \qquad \tau_\mathrm{n} = \tau_\mathrm{p} = \tfrac{1}{2}\tau , \qquad \boldsymbol{J}_\mathrm{n} \times \boldsymbol{J}_\mathrm{p} = \tfrac{1}{2}\boldsymbol{J} . \tag{II.40}$$

Then the energy density simplifies to

$$H(r) = \hbar^2\tau/2m + \tfrac{3}{8}t_0\rho^2 + \tfrac{1}{16}t_3\rho^3 + \tfrac{1}{16}(3t_1 + 5t_2)\rho\tau + \tfrac{1}{64}(9t_1 - 5t_2)(\nabla\rho)^2 - \tfrac{3}{4}W_0\rho\nabla\cdot\boldsymbol{J} . \tag{II.41}$$

In nuclear matter $\nabla\rho = 0 = \nabla\cdot J$, $\rho = \frac{2}{3}k_\mathrm{F}^3/\pi^2$, and $\tau = \frac{3}{5}k_\mathrm{F}^2\rho$. Then the binding energy per particle is

$$E/A = H/\rho = \tfrac{3}{5}E_\mathrm{F} + \tfrac{3}{8}t_0\rho + \tfrac{1}{16}t_3\rho^2 + \tfrac{3}{80}(3t_1 + 5t_2)\rho k_\mathrm{F}^2 \tag{II.42}$$

and the potential is

$$U(\boldsymbol{r}) = \tfrac{3}{4}t_0\rho + \tfrac{3}{16}t_3\rho^2 + \tfrac{3}{80}(3t_1 + 5t_2)pk_\mathrm{F}^2 . \tag{II.43}$$

Note that the potential and the energy density are related by $U = (\partial H/\partial\rho)_\tau$.

For colliding relativistic nuclei in the non-ultra-relativistic case, we can to first order neglect the problems of the relativistic field and calculate the potential locally. In the spirit of the Skyrme interaction in nuclear matter, we take the potential in a density expansion $U = a\rho + b\rho^2$ so that the binding energy is $E/A = \frac{3}{5}E_\mathrm{F} + \frac{1}{2}a\rho + \frac{1}{3}b\rho^2$. The long range Coulomb and Yukawa interaction are

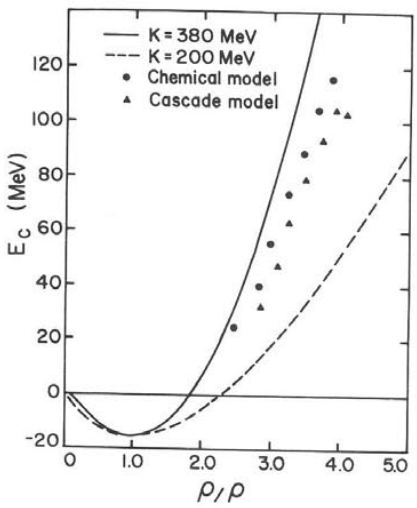

Fig. II.3. The Skyrme equations of state with $K = 200$ MeV and $K = 380$ MeV as used in the VUU theory [Kru85] are compared with values extracted from pion yields [Sto82].

neglected here; they become increasingly important at lower bombarding energies and for fragments emitted in the projectile and target rapidity region. We now measure ρ in units of $\rho_0 = 0.17/\text{fm}^3$. Then we impose the three conditions $E/A = -16$ MeV, $\frac{3}{5}E_F = 23$ MeV, and $K = 380$ MeV. The saturation condition $\partial(E/A)/\partial k_F = 0$ is equivalent to the zero pressure condition that $P = \rho^2 \partial(E/A)/\partial\rho = 0$ and the compressibility $K = k_F^2 \partial^2(E/A)/\partial k_F^2$ may also be written as $K = 9\rho\partial P/\partial\rho$. The three conditions (two are sufficient) fix the parameters $a = -124$ and $b = 70.5$. Similarly, if we take the expansion $U = a\rho + b\rho^{7/6}$ and impose $K = 200$ MeV, we find $a = -356$ and $b = 303$.

In fig. II.3, we plot these two local Skyrme interactions and compare to the equation of state extracted recently from pion multiplicity data [Sto82]. Note that the cascade and chemical model analysis, which extract a nuclear EOS from the differences of the calculated pion multiplicities and the observed pion yields, agree rather closely with our stiff EOS.

II.1.5. Application of the VUU theory — Study of the non-equilibrium and quantum effects

The VUU equation is difficult to solve since it is a highly non-linear differential equation in six dimensional phase space. The semi-classical character of this equation does allow one to solve it in terms of quasi-particles whose mean positions are solutions of Newton's equations [Kru85ab, Ber84ab, Mol84b, Mol85a, Mol85b]:

$$\boldsymbol{p}/m = \mathrm{d}\boldsymbol{r}/\mathrm{d}t \qquad \text{and} \qquad \mathrm{d}\boldsymbol{p}/\mathrm{d}t = -\partial U/\partial \boldsymbol{r}\,. \tag{II.44}$$

One does actually go beyond the VUU equation by including not only a mean field and Pauli blocking of the final state, but also relativistic kinematics and particle production.

The stability of the ground-state nuclei in this VUU theory is an important issue to address in testing the method [Mol86]. In fig. II.4, we show that the ground-state nuclei are quite stable up to times of the order of 80 fm/c.

To solve the VUU equation 15–100 collision simulations are followed in parallel and the ensemble averaged phase space density in a sphere of radius 2 fm around each particle is computed [Kru85a]. The ensemble averaging results in statistical fluctuations at the 10% level (at normal density) and thus reasonably smooth single particle distribution functions, which are used to determine the mean field and the Pauli blocking probability.

A constant time-step integration routine is used to insure synchronization of the ensembles. The acceleration of the test particles due to the field gradient is calculated prior to each transport step, and is assumed to be constant within a synchronization time-step. The local gradient of the field is computed via a finite difference method between two hemispheres centered around the test particle. This method is analogous to Lagrange's method in fluid dynamics, in contrast to the space-fixed Eulerian mesh.

Protons, neutrons, deltas and pions of different isospin are included separately with their experimental scattering cross sections. The question of double counting of the mean field and the collision term is a basic restriction for the VUU approach. We take the following operational point of view: the phenomenological Skyrme potential incorporates the real part of the potential, i.e. the attractive one meson exchange (the linear term in U) and repulsive mean field interactions, while the two body scattering accounts for the residual interactions. It should be pointed out that energy and momentum conservation is fulfilled in the present approach for individual two body scatterings and for the ensemble average on the mean (but not within each separate ensemble, because of the coupling between different ensembles — energy conservation problems have been studied for a similar approach

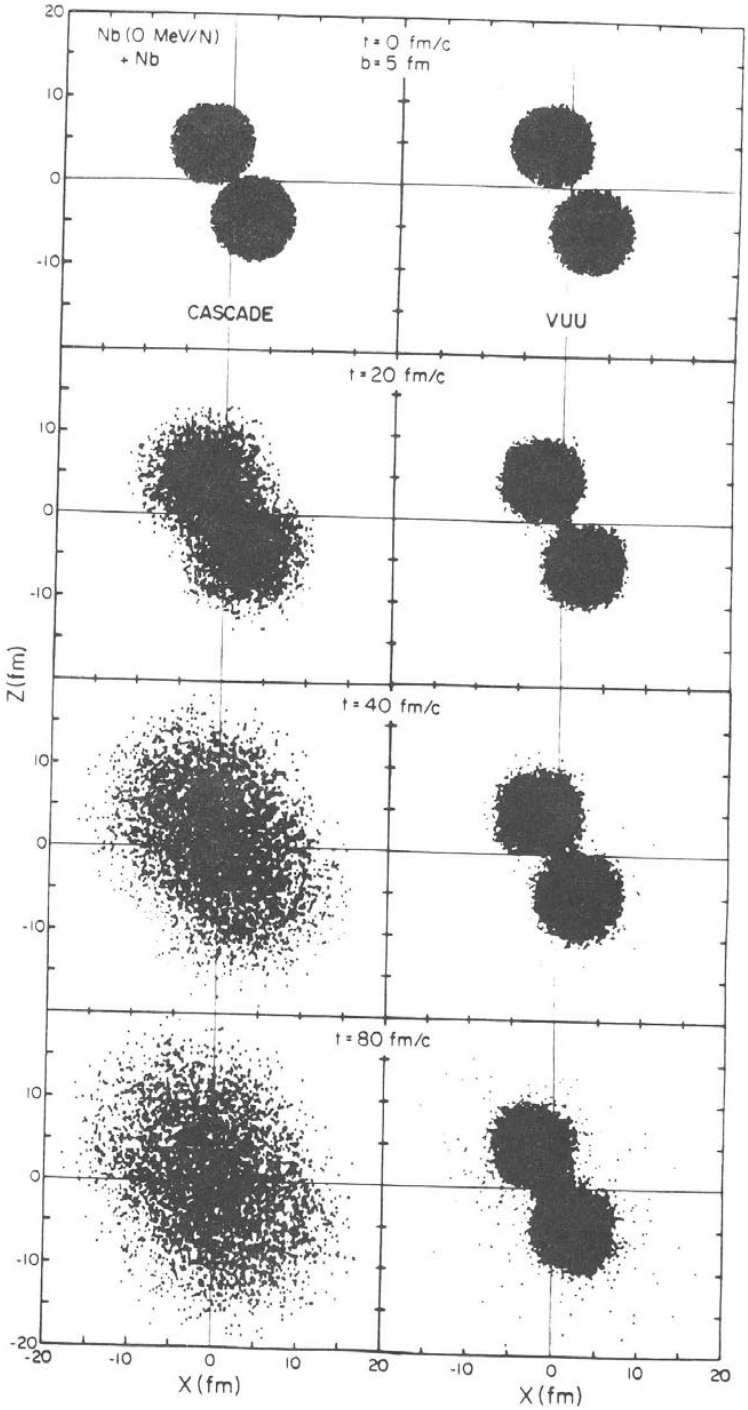

Fig. II.4. The stability of nuclei in the VUU approach versus a corresponding instability in the Cugnon cascade for Nb (0 MeV/nucleon) + Nb [Mol85].

by Koehler et al. [Koe80] using the relaxation time ansatz). The free particle cross sections have to be corrected for "in medium" effects, the most important one being the Pauli blocking of collisions. Two particles may undergo s-wave scattering if they approach each other with a minimum distance of less than $(\sigma/\pi)^{1/2}$ and if the final states are not Pauli blocked. The Pauli blocking factor for each nucleon is given by $(1-f)$, and the scattering probability is then reduced by the Uehling–Uhlenbeck factor $(1-f_1)(1-f_2)$. The Pauli blocker has been tested on ground state nuclei and has an efficiency of about 97%.

The Pauli blocking is very important even at intermediate bombarding energies: at 137 MeV/N, 80% of the attempted collisions are blocked due to lack of available final state configurations (fig. II.5). Many of these attempted collisions are between nucleons of the same nucleus. The spectra of low energy ($E < 80$ MeV) nucleons are also influenced by Pauli blocking.

What is the effect of the collision term in the VUU theory? The system Ar + Ca has been studied in the mean field approximation without two body collisions, thus mimicking TDHF by solving the Vlasov equation – as far as we know this is the first time that a solution of the Vlasov equation in three dimensions has been done for nuclear collisions. The lack of two body collisions results in strongly forward peaked angular distributions, in qualitative agreement with 3D TDHF calculations [Stö80] in this energy regime. Figure II.6a shows the initial state in momentum space for Ar (137 MeV/N) + Ca; note that at this energy the Fermi spheres of target and projectile nuclei are well separated. The Ar projectile moves in the positive z-direction, while the Ca target moves in the negative z-direction in this center of mass frame. Figures II.6b, c show the final state of this reaction as obtained in the present theory without and with the Uehling–Uhlenbeck collision term. Note that the momentum space distribution is practically unchanged in the mean field calculation – equilibration of the momenta is not observed – while the inclusion of the Uehling–Uhlenbeck collision term results in strong equilibration – the isotropy in fig. II.6c is indicative of substantial thermalization. A convenient way to compare the results is to use the ratio of transverse to longitudinal momenta

$$R = \frac{2}{\pi} \sum p_{\text{per}} \Big/ \sum p_{\text{par}} \,. \tag{II.45}$$

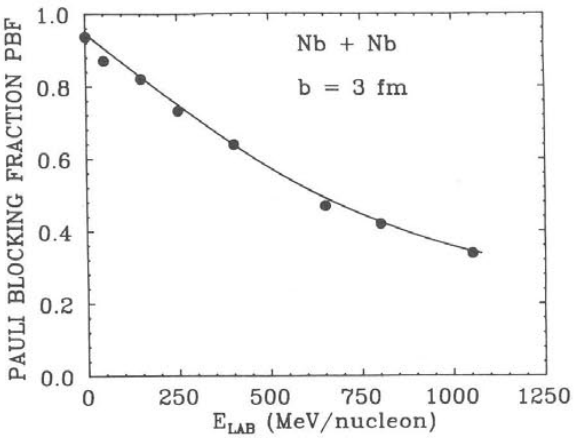

Fig. II.5. Fraction of Pauli-blocked collisions in the VUU theory versus energy for the Nb + Nb system at $b = 3$ fm [Mol85].

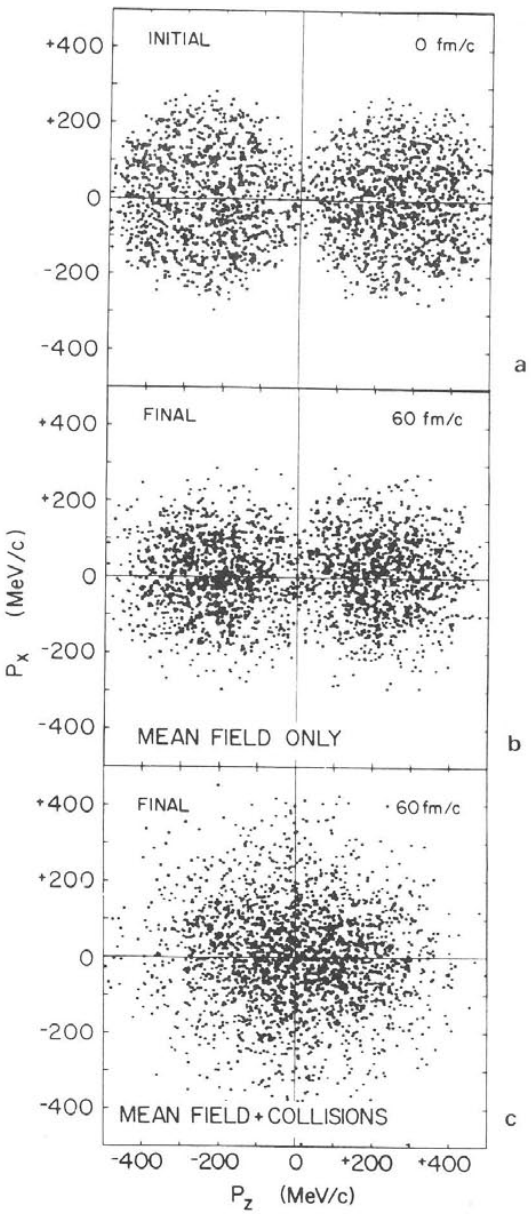

Fig. II.6. The evolution in momentum space in the VUU theory of Ar (137 MeV/nucleon) + Ca at $b = 0$ fm. The results from several parallel ensembles are superposed in order to represent the distribution function. The collision term results in substantial equilibration [Kru85b].

where p_{per} and p_{par} are the momenta perpendicular to and parallel to the beam. Comparing the ratio of final to initial R values, one finds 1.08 for the mean field only case and 2.05 for the mean field + collisions approach [Kru85b]. At lower energies, the comparison is not as dramatic; the initial R values are already high since the nuclei overlap more in momentum space – furthermore, most of the collisions are Pauli blocked. But the collision term always leads to increased isotropy. In configuration space, one finds the well known transparency when the Vlasov equation is solved and some stopping

when the collision term is included: a substantial degrading of the initial momentum occurs once the collision term is included [Kru85b, Aic85].

Figure II.7 shows for C (85 MeV/nucleon) + C at $b = 1$ fm the time evolution in configuration space in the three dimensional TDHF and Vlasov equation calculations [Aic85]. There is a very similar behavior in both the quantum mechanical and classical mean field theories: both calculations exhibit transparency and nearly identical small longitudinal and transverse momentum transfers. The lack of two body collisions results in strongly forward peaked angular distributions, in sharp contrast with the data in this energy regime. Both theories predict that for central collisions of C + C the nuclei slip through each other

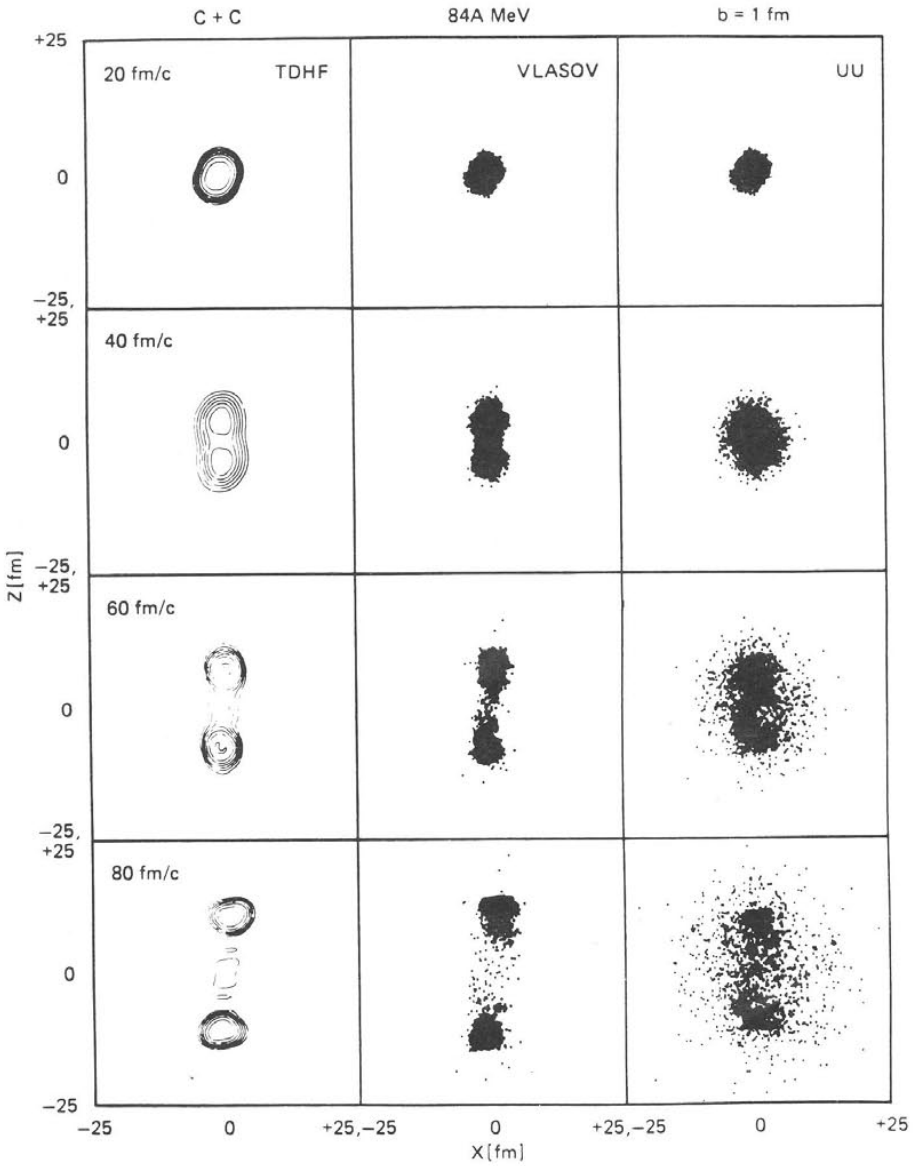

Fig. II.7. Time evolution in configuration and momentum space for C (85 MeV/nucleon) + C at $b = 1$ fm for TDHF, the Vlasov equation, and the Vlasov–Uehling–Uhlenbeck theory. Transparency occurs in both cases with a mean field only [Aic85].

and survive the reaction rather intact. About 85% of the initial longitudinal momentum is conserved in the projectile- and target-like nuclear fragments. Hence the low angular momentum fusion window previously observed in TDHF calculations persists up to energies of 85 MeV/N. The TDHF calculations require more than an order of magnitude more computing time than the Vlasov approach.

The inclusion of the Uehling–Uhlenbeck collision integral into the Vlasov equation changes this drastically (fig. II.7): each individual reaction can now be separated into two clearly distinct components. First, we observe again the slipped-through projectile- and target-like fragments which, however, now retain only about 40% of the nucleons and less than 20% of the initial longitudinal c.m. momentum. As we see in fig. II.7, these slipped-through residues contain mostly particles which have not scattered at all.

The second component consists of 60% of the projectile nucleons which underwent at least one nucleon–nucleon scattering and form a non-equilibrated mid-rapidity system, which shows an almost isotropic emission pattern. It is interesting to note that projectile or target residues are not observed in the VUU approach if heavier symmetric systems are studied, e.g. for Ca + Ca at bombarding energies from 40 to 140 MeV/nucleon [Kru85]. At even higher energies, Ar (800 MeV/N) + Pb, complete stopping of the projectile in the target has been predicted [Mol85b, 86]. What is then the reason for the incomplete deceleration of the nuclei in the above study? At these low energies we observe that a large fraction of the attempted nucleon–nucleon collisions is forbidden by the Pauli blocking of the exit channels. Thus the nucleon's mean free path is effectively longer as a result of the Pauli principle. Furthermore, the C–C system is rather small, hence the chances for a nucleon–nucleon collision to occur is smaller than in a bigger system.

At less central impact parameters, negative angle scattering is observed in both pure mean field approaches, and again the classical and the quantum approach agree remarkably well. The collision term results in less inward scattering. The mid-rapidity source is much less apparent; two slightly decelerated and excited residues survive the collision. The effect of the collision term is less dramatic at these larger impact parameters due to the smaller geometrical overlap of the nuclei, which reduces the number of nucleon–nucleon collisions even more.

A generalized 6-dimensional coalescence model may be used to find the nucleons bound in clusters, and prevent them from contributing to the calculated proton cross sections [Kru85b]. This is important at medium energies, where a large fraction of the emitted protons are found to be bound in fragments. In this scheme, a nucleon is part of a cluster if it is within a configuration space distance r_0 from any other member of the cluster, and within a momentum space distance p_0 from the center of momentum of the cluster. The sequential evaporation of protons from residual fragments is not included. The generalized coalescence prescription has been used to calculate inclusive proton spectra from the primordial nucleon distribution. We show below the results for $r_0 = 2.2$ fm and $p_0 = 200$ MeV/c. These parameters are adjusted to agree with the experimentally observed total cross sections. These values also yield correct clustering at $t = 0$ fm/c: two heavy clusters, namely the ground state nuclei, are then obtained. Variation of the coalescence parameters changes the magnitude of the cross sections, but has a negligible effect on the shape of the spectra. It is interesting to point out that the phase space volume spanned by these values is very close to $4h^3$, the volume occupied by a fourfold degenerate Fermion. Our approach gets further support from the agreement of the predicted fragment yields as a function of fragment mass to the experimental data for masses 1–14 [Jac83].

Figure II.8 shows the comparison between calculated and measured proton spectra for 42 and 92 MeV/N Ar + Ca. The calculated absolute cross sections and the slopes of the spectra agree reasonably well with the data. In contrast, a simple cascade simulation, though appropriate for high energies, cannot reproduce the medium energy data.

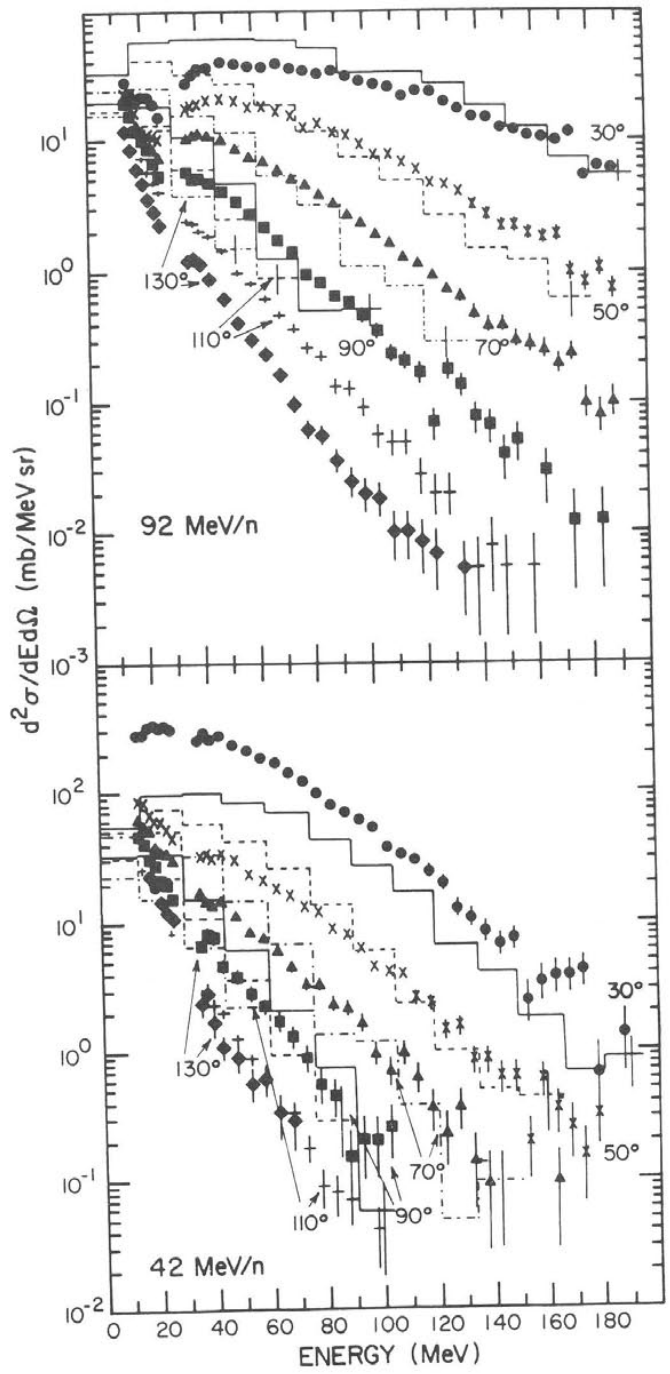

Fig. II.8. Single particle inclusive proton spectra experimentally and theoretically (histograms) in the VUU theory for the Ar + Ca system [Kru85b].

In fig. II.9 we show the reaction C (85 MeV/N) + C at $b = 1$ fm in more detail [Aic85]. We display the initial and the final density profiles in configuration and momentum space. For the display of the final state particles which did not undergo any collision ($N_c = 0$) and scattered particles with $N_c > 0$ have been distinguished. The projectile-like fragments contain on the average 3–4 unscattered nucleons and

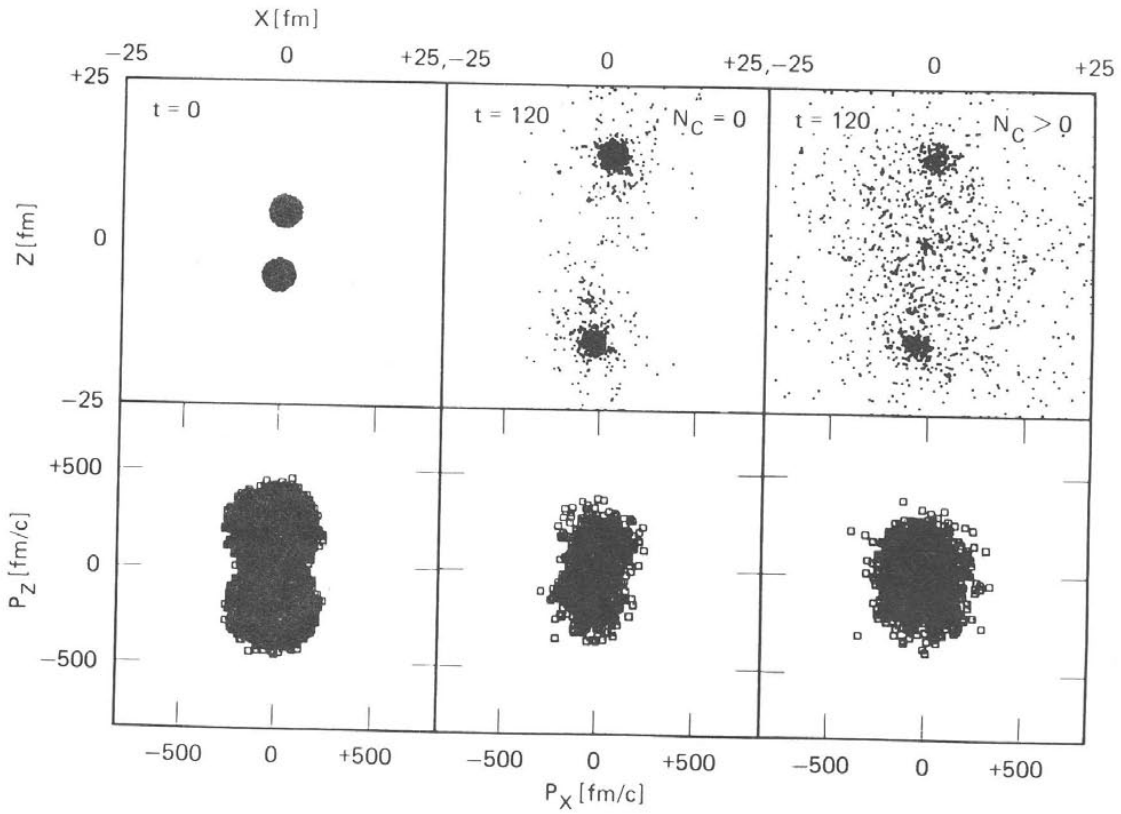

Fig. II.9. Initial and final states in configuration and momentum space in the VUU theory for C (85 MeV/nucleon) + C at $b = 1$ fm [Aic85].

about 1–2 scattered nucleons get trapped by the attractive mean field of the projectile-like fragment. The mid-rapidity region contains almost exclusively scattered particles. The high momentum components of the initial momentum space distribution get most effectively depleted by collisions because for them the Pauli blocking is least effective. The projectile-like fragments have densities around $\rho_0/2$. Hence their Fermi energy is lowered. A collective deceleration of these projectile-like fragments is caused by the mean field. Those particles which have undergone collisions exhibit a nearly isotropic distribution in momentum space, with some forward–backward asymmetry.

The dependence of the nuclear stopping power on the target mass has also been studied [Aic85]. To accomplish this goal, central collisions of ^{12}C (85 MeV/nucleon) projectiles with 6 different targets from ^{12}C to ^{197}Au have been studied. The number of projectile nucleons undergoing at least one collision increases from about 60% for the C target to about 97% for the Au target. These collisions result in a momentum transfer on the target-like residue of 44 MeV/(c nucleon) (66% of the maximum momentum transfer possible, 67 MeV/(c nucleon)) for Ni targets to 18 MeV/(c nucleon) (80% of the maximum 22 MeV/(c nucleon)) for Au targets. For the heavier targets ($A_T > 50$) this goes hand in hand with an almost complete stopping of the projectile in the target. This result is similar to what has been obtained with the VUU method for $^{40}Ar + {}^{197}Au$ at 92, 400 and 800 MeV/nucleon bombarding energy [Mol86]. The number of projectile nucleons being emitted without having had a collision up to a time $t = 160$ fm/c is shown in fig. II.10 as a function of the target diameter D_t for 100 parallel runs each. Observe the exponential falloff of N_0 with D_t. This can be reproduced by assuming that the mean free path

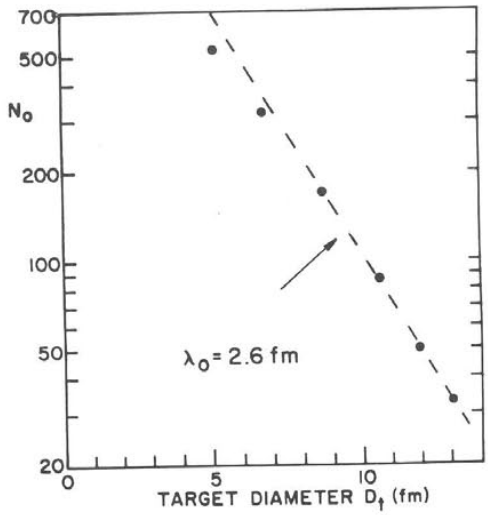

Fig. II.10. The number of uncollided projectile nucleons in the VUU model emitted for C (85 MeV/nucleon) induced reactions is used to extract a mean free path [Aic85].

of the nucleons in heavy ion collisions in this energy region is $\lambda = 2.6$ fm. This value is larger than the mean free path estimated from classical kinetic theory, $\lambda_c = (\sigma\rho)^{-1/2} = 1.4$ fm. This discrepancy is mainly due to the effects of the Pauli principle, which blocks a fraction of the attempted collisions in the VUU approach in accord with the local phase space density. Other effects which contribute are the density increase in the collision (which decreases λ) and the finite deceleration due to the mean field (which also decreases λ). Please note that for C and Al targets we observe projectile remnants surviving the interaction. Because of residual collisions within these final clusters – after the clusters have separated – we expect N_0 to be smaller than what is expected from the extrapolation from the heavier targets. This is indeed observed.

Let us examine the evolution of the single particle distribution function as obtained from the VUU approach for Ar (770 MeV/N) + Pb collisions. In figs. II.11 and 12 we display projections of the distribution function into configuration and momentum space for this system. (Note that for ease of viewing, we have flipped both the x and z axis in the configuration space plots and also the p_z axis in the momentum space plots.) The collision term is essential at both intermediate and high energies, as one expects intuitively. Note in figs. II.11 and 12 that at low impact parameter the Ar projectile is completely consumed by the Pb target in configuration- as well as in momentum space. The $t = 0$ configuration space plots show the correct nucleon–nucleon center of momentum frame Lorentz length contraction by a factor $1/\gamma = 0.85$. In configuration space, for $t = 10$ fm/c, the squashed elliptical to octupole shape is an indication of the high density formed in these collisions. For example, at 1 fm impact parameter, the density within a sphere of radius 2 fm centered at the origin reaches $2.7\,\rho_0$ at 5 fm/c time; then, the density falls very rapidly – by 17 fm/c it is below the ground-state value. The directed sidewards flow of nucleons is easily seen in configuration space at $b = 3$ and 5 fm by the excess of nucleons in the quadrant with $x < 0$ and $z < 0$ (as opposed to $x < 0$ and $z > 0$) as early as $t = 20$ fm/c. Spectator fragments are also observed, namely at 5 fm. The projectile is seen to not just shear off the target; it rather experiences a substantial transverse momentum transfer away from the region of high density – the bounce-off effect predicted earlier on the basis of nuclear fluid dynamics [Stö80b, Buc83a,b]. Thus simple geometric models can only be a very rough approximation to the more complicated reaction dynamics illustrated here.

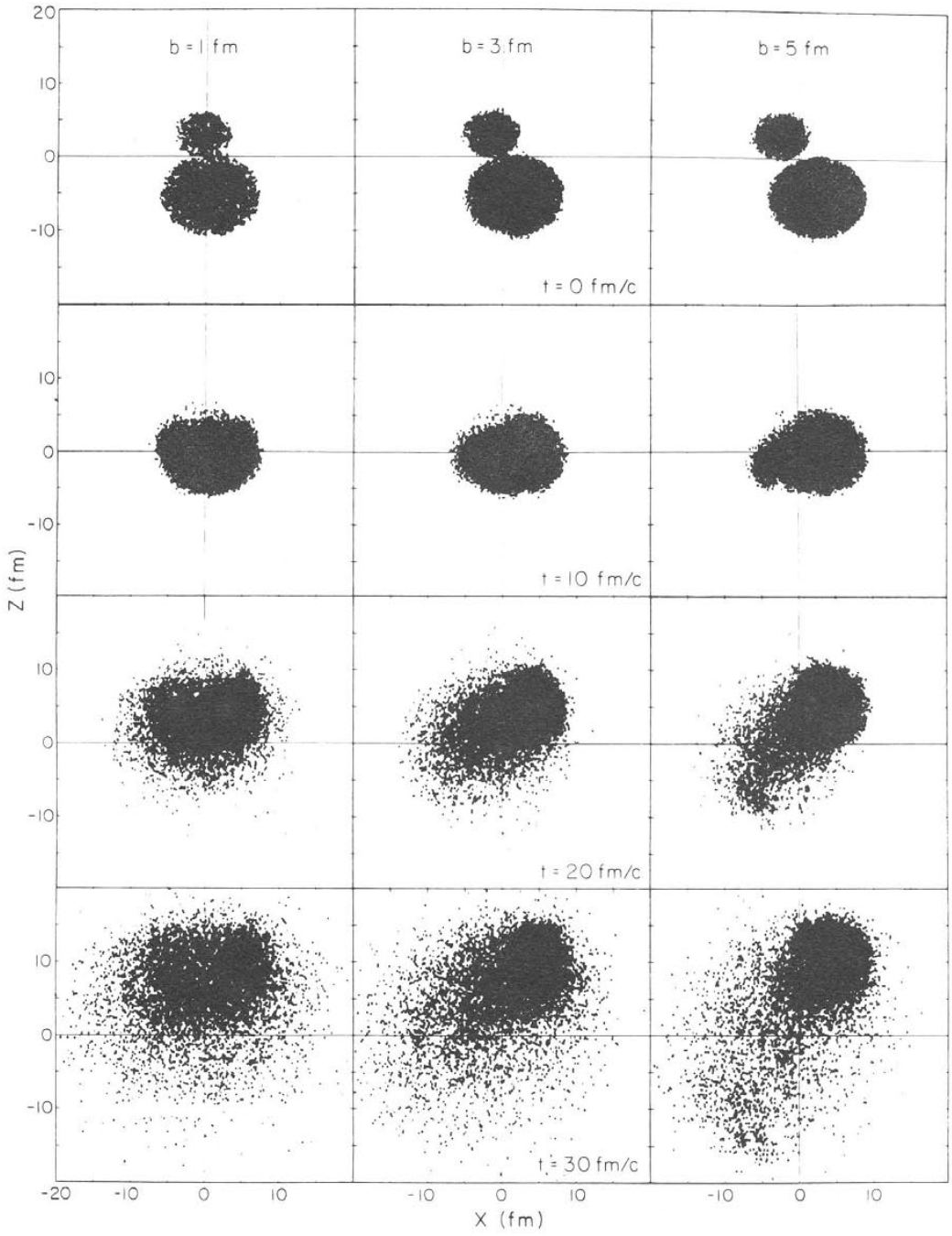

Fig. II.11. The time evolution of the single particle distribution function as obtained in the VUU theory for Ar (770 MeV/nucleon) + Pb is shown after projection into configuration space at $b = 1, 3$ and 5 fm [Mol85].

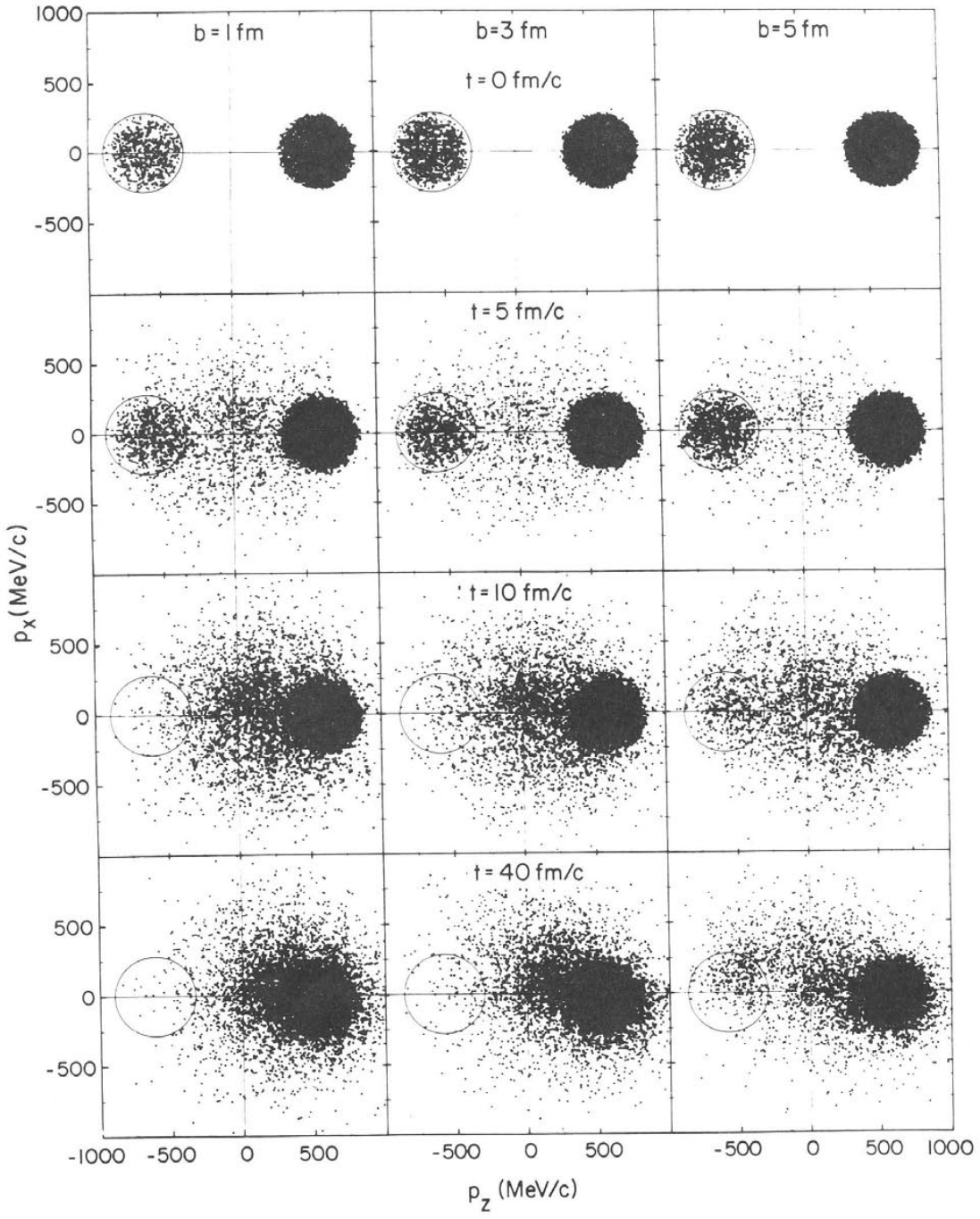

Fig. II.12. The time development of the same system after projection in momentum space [Mol85]. The rapid (t = 10 fm/c) equilibration is obvious for near central collisions.

The momentum space evolution of the single particle distribution function displayed in fig. II.12 exhibits rapid equilibration at low impact parameters: observe that the projectile sphere in momentum space is rapidly depopulated by two body collisions at $b = 1$ and 3 fm. At $t = 5$ fm/c substantial filling of the nucleon–nucleon center of momentum region is observable, signaling the formation of a participant zone. At $t = 10$ fm/c, there are practically no nucleons left in the originally densely populated projectile momentum sphere; almost all of the projectile nucleons have been scattered out of their initial momentum states. At $b = 1$ fm, this scattering has been with about equal probability into the positive and negative p_x direction. At $b = 3$ fm, a preference for the positive p_x direction can clearly be observed – this is due to the expansion of the compressed participant matter away from the high density repulsive interaction into the vacuum. At $t = 40$ fm/c the number of hard nucleon–nucleon collisions has become negligible, the final state in momentum space is closely approached. Observe that secondary, tertiary, etc. collisions of the participants with the target spectator have resulted in a further decrease of the number of fast particles and in a more diffuse momentum distribution in the projectile hemisphere, with a very pronounced sidewards flow visible at $b = 3$ fm.

At the intermediate impact parameter, $b = 5$ fm, the situation is even more complicated: since projectile and target exhibit only about half overlap, there are a substantial number of projectile nucleons which do not experience collisions with the target nucleons. Hence the depopulation of the projectile momentum sphere is incomplete, part of the projectile is stopped and forms the participant zone together with the struck nucleons from the target, while the projectile spectators move ahead with nearly their initial longitudinal momentum. The behavior of the participant nucleons is nearly the same as at the lower impact parameters – equilibration is achieved rapidly ($t = 10$ fm/c) and sidewards flow is observed. The projectile nucleons which have not undergone collisions, and thus the projectile-like fragments formed from them, exhibit a finite transverse momentum transfer into the same direction as the directed participant side splash. This bounce-off of the participants is a result of the repulsive interactions felt by the spectators in the vicinity of the compression zone. The simultaneous occurrence of this bounce-off and the sidesplash has recently been experimentally observed [Gus84] in symmetric systems with high statistical confidence. A theoretical analysis of these processes for symmetric systems is presently underway [Mol85b].

The equilibration at low impact parameter goes hand in hand with nuclear stopping; without the collision term, the nuclei are transparent. As a reference case, we have also solved the Vlasov equation by turning off the collision term; then the final momentum distribution looks very much like the initial one, as is the case also at lower energies. An easily accessible experimental quantity is the longitudinal momentum p_z in the laboratory frame. The multiplicity dependence of this quantity should give information on the nuclear stopping. Note that initially the Ar nuclei form a bump at the beam momentum whereas the Pb nuclei are at rest. In the final state at the lower impact parameter we see evidence of nuclear stopping: there is no projectile remnant and the Pb target is accelerated. At the higher impact parameter, there is less stopping: one sees some projectile remnants and the target-like fragments are accelerated less [Mol84b].

II.1.6. Intranuclear cascade simulations and their limitations

The intranuclear cascade model represents the limit of the VUU theory where there is no binding mean field, no sophisticated Pauli blocking. Historically, the intranuclear cascade idea is due to Serber [Ser47]. His idea was that nuclear reactions at high energies might be understood in terms of a quite simple picture different from the description needed at low energies. Because the collision time between

an incident high energy nucleon and a nucleon in the nucleus is short compared to the time between collisions of the nucleons in the nucleus, he inferred that the high energy reaction could be modelled as a cascade process. Collisions occur between the incident particle and those particles which are directly struck in the nucleus. This model was first investigated in two dimensions in 1948 by Goldberger [Gol48] who performed his calculations by hand for the case of high energy neutrons interacting with heavy nuclei. The first fully three dimensional calculations were done by Metropolis et al. in 1958 [Met58] for incident protons and neutrons using the MANIAC computer; they also added a second stage to the cascade calculation during which the excited residual nucleus evaporates particles, as had also been suggested by Serber.

Many others have contributed to the development of the intranuclear cascade model. The two most commonly used versions of the cascade code in the theory of high energy heavy ion reactions are due to Yariv and Fraenkel [Yar79, 81] and Cugnon et al. [Cug80–84]. What is the intranuclear cascade model as it is used in these codes? It is a microscopic simulation of a nuclear reaction at high bombarding energies. Nuclear collisions are treated as a superposition of independent two body nucleon–nucleon collisions. Nucleons move on straight line trajectories (since there is no field) until they collide with a probability given by the free nucleon–nucleon scattering cross section. The creation of deltas, pions, and other particles and the interaction of all these particles occurs according to experimental cross sections. The intranuclear cascade models incorporate relativistic kinematics. Target and projectile nucleons are initialized in configuration and momentum space with random Fermi momenta and then Lorentz boosted to an appropriate frame, where the collision simulation proceeds. Momentum and energy are conserved in the particle–particle interactions and the evolution of the system is followed up to a time where the majority of interactions have ceased. Collisions are only Pauli blocked according to a simple criterion, say if the total center of mass energy is less than the Fermi energy in ground state nuclear matter or if the outgoing particle would scatter into momentum space regions originally occupied by projectile or target.

Both the Yariv–Fraenkel and the Cugnon cascade satisfy the above criteria. They differ in two respects: (1) the particles in the Yariv–Fraenkel simulation sit in a potential well of constant depth V_0; (2) in the original Yariv–Fraenkel approach the incoming particles (projectile nucleons) are cascading independently through a medium (the target). In the updated version, this scheme has been improved by including the so-called cascade–cascade interactions – for a given cascade particle (a particle which has undergone at least one collision) the other cascade particles are acting as a medium superimposed on the original target medium.

In the Cugnon cascade, one has the problem that the nucleons are not bound; hence one may get spurious effects due to nuclear instability, see fig. II.4 [Mol86]. It is possible to bind the nucleons by letting each nucleon move only with the beam velocity until it interacts with another nucleon, at which point it 'remembers' it's Fermi momentum. Note however that the bound Cugnon cascade is theoretically not very satisfying either, since in real nuclei, nucleons can travel in all directions.

II.2. Nuclear fluid dynamics

II.2.1. Conservation laws and the transition to local equilibrium

Just as in the classical case, one can derive from the VUU equation a general transport equation for a function f [Mar85, Mol85]. Assume for simplicity that the external force $\boldsymbol{F} = \mathrm{d}\boldsymbol{p}/\mathrm{d}t$ is momentum independent. Let us also re-write the VUU equation in the simple form: